Global Analysis of Storm Surge Seasonality

Apolola, Ayoola; Ward, Philip J.; Tiggeloven, Timothy; Antolínez, José A. Á. ; Jäger, Wiebke; Muis, Sanne

DOI
10.1029/2025JC022841

Publication date
2025

Document Version
Final published version

Published in
Journal of Geophysical Research: Oceans

Citation (APA)
Apolola, A., Ward, P. J., Tiggeloven, T., Antolínez, J. A. Á., Jäger, W., & Muis, S. (2025). Global Analysis of Storm Surge Seasonality. *Journal of Geophysical Research: Oceans*, *130*(11), Article e2025JC022841. https://doi.org/10.1029/2025JC022841

JGR Oceans

RESEARCH ARTICLE

10.1029/2025JC022841

Global Analysis of Storm Surge Seasonality

Ayoola Apolola[1], Philip J. Ward[1,2], Timothy Tiggeloven[1], José A. Á. Antolínez[3], Wiebke Jäger[1], and Sanne Muis[1,2]

[1]Institute for Environmental Studies (IVM), Vrije Universiteit Amsterdam, Amsterdam, The Netherlands, [2]Deltares, Delft, The Netherlands, [3]Department of Hydraulic Engineering, Faculty of Civil Engineering and Geosciences, Delft University of Technology, Delft, The Netherlands

Key Points:

- Storm surge seasonality from 1980 to 2018 was based on surge data from the global tide and surge model
- The assumption of a unimodal storm surge season does not apply to nearly half of the global coastal stations
- Tropical and subtropical regions exhibit bimodal surge seasons tied to large-scale regional atmospheric patterns

Supporting Information:

Supporting Information may be found in the online version of this article.

Correspondence to:

A. Apolola,
a.c.apolola@vu.nl

Citation:

Apolola, A., Ward, P. J., Tiggeloven, T., Á. Antolínez, J. A., Jäger, W., & Muis, S. (2025). Global analysis of storm surge seasonality. *Journal of Geophysical Research: Oceans*, *130*, e2025JC022841. https://doi.org/10.1029/2025JC022841

Received 5 MAY 2025
Accepted 20 OCT 2025

Author Contributions:

Conceptualization: Ayoola Apolola, Philip J. Ward, José A. Á. Antolínez, Wiebke Jäger, Sanne Muis
Data curation: Ayoola Apolola, Sanne Muis
Formal analysis: Ayoola Apolola
Funding acquisition: José A. Á. Antolínez, Sanne Muis
Investigation: Ayoola Apolola, Philip J. Ward, Timothy Tiggeloven, José A. Á. Antolínez, Wiebke Jäger, Sanne Muis
Methodology: Ayoola Apolola, Philip J. Ward, Timothy Tiggeloven, Wiebke Jäger, Sanne Muis
Project administration: José A. Á. Antolínez, Sanne Muis
Software: Ayoola Apolola

Abstract We perform the first global analysis of storm surge seasonality using surge data from a global hydrodynamic model with full coverage of coastal areas, providing valuable insights for regions not represented in alternative observational data sources. We apply directional statistics based on the mixture model of the von Mises-Fisher distribution to identify surge seasons and their characteristics. Results reveal that nearly half of the global coastal stations, predominantly in tropical and subtropical regions, either lack a distinct surge season or experience heightened surge activity across multiple periods. Furthermore, the seasonality of storm surges follows a consistent large-scale spatial pattern tied to regional atmospheric variables. Spatial variability in the length of surge seasons is minimal in regions with bimodal surge seasons; however, the variability of surge peaks differs. Lastly, the seasonal distribution of storm surges differs regionally due to the underlying storm regime. These results provide valuable insights into the seasonality of storm surges on a global scale, which is useful for coastal risk management.

Plain Language Summary Storm surges, the abrupt rise in sea levels above tidal elevations during a storm, are among the most devastating causes of coastal flooding globally. However, they are influenced by seasonal variations in atmospheric processes, which can amplify their peaks. In this study, we analyzed when these peaks typically occur and how the seasons vary spatially over a consistent period globally. By using surge data from a global hydrodynamic model with comprehensive geographical coverage, we provide insights for regions that lack observations from alternative data sources such as tide gauges. We show that the seasonality of surge peaks is not confined to a single well-defined season globally. Some regions lack clear seasons, while others have well-defined seasons with varying numbers. This means that some regions have more pronounced seasonal cycles than others. Despite this variation, the seasonal patterns are regionally coherent and are tied to underlying atmospheric patterns. Understanding these seasonal patterns could help improve coastal management plans, especially in places with extended surge risk windows.

1. Introduction

Storm surge is the anomalous rise in sea level above the predicted tide. It is driven by low air pressure and high wind speed associated with weather events such as midlatitude and tropical storms (Pugh & Woodworth, 2014). These surges can reach heights of several meters, especially in coastal areas with broad and shallow continental shelves (Mcinnes et al., 2003; Nicholls, 2006), posing significant environmental and socioeconomic threats when the resulting sea level overtops coastal defenses. Notable events such as Hurricane Katrina in the US, extratropical cyclone Gudrun in northern Europe, and cyclone Freddy in Mozambique demonstrate the potentially devastating impact of these events (Mäll et al., 2017; Mester et al., 2023; Petterson et al., 2006).

Understanding the variability of storm surges across different timescales is essential for effective coastal flood management and has implications for maintaining coastal defenses (Dhakal et al., 2015; Parajka et al., 2010; Trace-Kleeberg et al., 2023). Large-scale atmospheric processes influence surge variability from subseasonal to multidecadal timescales (Marcos et al., 2015; Wahl & Chambers, 2016), with seasons being a dominant feature (Tsimplis & Woodworth, 1994; Woodworth et al., 2019). Seasonality reflects the intraannual variations in the timing and frequency of storm surges.

Past studies have employed statistical models to examine the temporal variability of storm surges over different spatial extents (Calafat et al., 2022; Mawdsley & Haigh, 2016; Wu et al., 2017). The few large-scale studies on seasonality of extremes have typically used nonstationary extreme value models based on monthly maxima (Bij de Vaate et al., 2024; Lobeto et al., 2018; Reinert et al., 2021; Roustan et al., 2022). For instance, in a global study,

Supervision: Philip J. Ward, Timothy Tiggeloven, José A. Á. Antolínez, Wiebke Jäger, Sanne Muis
Visualization: Ayoola Apolola
Writing – original draft: Ayoola Apolola
Writing – review & editing: Ayoola Apolola, Philip J. Ward, Timothy Tiggeloven, José A. Á. Antolínez, Wiebke Jäger, Sanne Muis

Menéndez and Woodworth (2010) estimated that the timing of the highest 50-year return values coincides with the local storm season. More recently, Bij de Vaate et al. (2024) expanded on this work by analyzing surge peaks globally for return periods of 1/6 years and 10 years. Their findings further support the link between the timing of the highest surge peaks and the local storm season.

Moreover, past studies have relied on observational records from tide gauges or satellite altimeters (Barroso et al., 2025; Calafat et al., 2022; Mawdsley & Haigh, 2016; Wu et al., 2017). Tide gauge records generally provide the most accurate measure of sea level variability along coastlines. However, their spatial distribution is uneven, with most tide gauges concentrated in the Northern Hemisphere (Lobeto et al., 2018; Menéndez & Woodworth, 2010). In contrast to tide gauges, satellite altimeters provide global coverage. However, the temporal record of this data set is limited, as satellite records extend back to 1992 (Naeije, 2022). Moreover, satellite altimetry data have poor spatial resolution along coastlines (Fernández-Montblanc et al., 2020) and struggle to capture short-lived tropical storms (Bij de Vaate et al., 2024), making them less reliable for analyzing seasonality in tropical regions.

Due to the limitations of observational records, sea level data from global hydrodynamic models have emerged as a valid alternative for coastal studies (Dullaart et al., 2021; Muis et al., 2018, 2020; Rueda et al., 2017; Vousdoukas et al., 2018). The global tide and surge model (GTSM), for instance, provides consistent global time series of storm surges (Copernicus Climate Change Service [C3S] 2022). However, while time series derived from GTSM have been used to assess the frequency and magnitude of extreme sea levels (Dullaart et al., 2021; Muis et al., 2023), an analysis of the seasonality of storm surges is still lacking.

To close this knowledge gap, this study aims to investigate the seasonality of storm surges at the global scale. We leverage 39 years of surge data from the GTSM (Copernicus Climate Change Service [C3S] 2022), which provides full global coverage with consistent temporal records from 1980 to 2018. While previous global studies have used nonstationary extreme value statistics to evaluate in which month the highest storm surge occurs, we employ directional statistics (Jammalamadaka & Sengupta, 2001; Mardia & Jupp, 2009) to assess the number of storm surge seasons, their length, and the peak of the season. We also evaluate how the magnitudes of the seasonal surges vary regionally.

The rest of the paper is structured as follows. Section 2 describes the material and methods applied in our study. This section describes our surge data and provides a step-by-step application of our statistical approach. In Section 3, we present our results, focusing on the seasonality of extreme storm surges. In Section 4, we discuss our findings and their potential implications for coastal flood management.

2. Material and Method

Our approach consists of four main steps, as shown in Figure 1 and described in detail in Sections 2.1–2.4. In brief, the steps are as follows:

1. Data selection: First, we selected global surge data from the GTSM for 43,119 model output stations from 1980 to 2018.
2. Data preprocessing: Next, we conducted quality checks by dropping output stations with spurious surge peaks and corrected for meteorological trends in the time series of the remaining stations.
3. Assessing the magnitude of surge peaks: Subsequently, over the entire time series, we applied a spatially varying peak over threshold (POT) method to achieve an average of 3 events per year at each output station.
4. Assessing the seasonality of surge peaks: Lastly, we analyzed the seasonality of these peaks based on the mixture model of the von Mises-Fisher (vMF) distribution. The length of the identified seasons was determined from the first derivative of the distribution function

2.1. Data Description

We use hourly time series of surge levels from 1980 to 2018 obtained from the global tide and surge model (GTSMv3.0). The GTSM is a global depth-averaged hydrodynamic model developed using the unstructured Delft3D Flexible Mesh software (Kernkamp et al., 2011). Its spatial resolution increases from 25 km in the deep ocean to 2.5 km along the coastline. In Europe, the model resolution further increases to 1.25 km (Muis et al., 2020). GTSM simulates still water levels resulting from tidal and meteorological forcing, using 10 m wind speed and atmospheric pressure data from the ERA5 atmospheric reanalysis (Hersbach et al., 2020; Muis

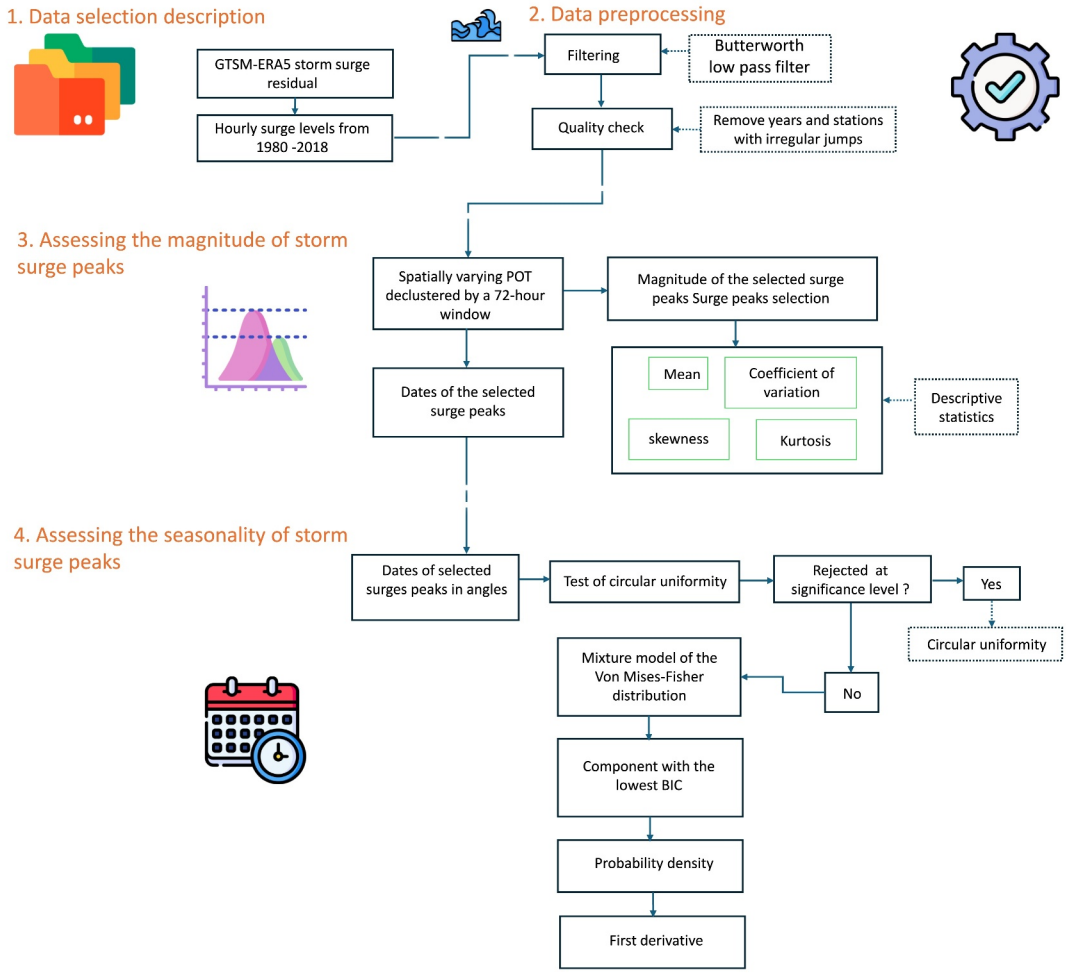

Figure 1. Flowchart showing the flow of the statistical framework adopted in this study.

et al., 2023). The GTSM-ERA5 data set provides water level time series for 43,119 output stations spanning the coastline and the deep ocean (Copernicus Climate Change Service [C3S] 2022). GTSM-ERA5 has been extensively validated in previous studies (Dullaart et al., 2020; Muis et al., 2016). Although it tends to underestimate tropical cyclone (TC) intensity due to spatial and temporal forcing, it generally shows good agreement between modeled and observed surge levels.

2.2. Data Preprocessing

We start the data preprocessing with a quality check on the surge level time series for all output stations. We inspect output stations with surge levels (outliers) exceeding 9 m, which corresponds to the storm surge height recorded during Hurricane Katrina, the highest between 1980 and 2018 (Needham & Keim, 2012; Weather Underground, 2025). Based on this criterion, we identified five output stations with spurious peaks, all located in areas of complex bathymetry or inside estuaries, which the GTSM cannot fully resolve. We exclude those five stations (about 0.01% of the total output stations) from our analysis. We also review stations with surge peaks up to 5 m, but this did not lead to the exclusion of more stations. There may still be stations containing outliers, but given the small number of stations, we do not expect this to have any significant effect on the overall analysis. In addition, we verify that the remaining output stations have surge values for 99.99% of their time steps and exclude time steps with missing values from our time series.

After the quality checks, we remove the low-frequency signal corresponding to the annual variation in surge levels, using the 2nd-order Butterworth low-pass filter (Roberts & Roberts, 1978). We do this to eliminate the influence of long-term meteorological trends, such as variations in the pressure and wind patterns that affect mean sea level variations but are not associated with extreme events (Hermans et al., 2020; Lowe et al., 2021) and instead focus on surge peaks from extreme events. The filtering parameters are set as follows: (1) the sampling rate and the cutoff frequency are set to hourly and annually, matching the temporal resolution of our data and the annual surge level frequency, respectively; 2) the Nyquist frequency, which is used to normalize the cutoff frequency, is set to half the sample rate; and (3) the order number is set to two.

We test the filter's sensitivity to higher-order numbers (3 and 4) and find negligible differences in the result. While higher-order filters can better address edge effects in the low-frequency signal, they tend to introduce more pronounced phase distortion. Therefore, we use the 2nd-order filter to balance simplicity and minimize phase distortion in the low-frequency signal. Additionally, we use the 2nd-order Butterworth low-pass filter instead of the moving average approach to prevent distorted trends or lags in the time series (Parker et al., 2023). Figure 2 below compares both approaches for selected locations. Note that the moving average was centered on an annual window of 8,766 hr, which shifts forward by 1 hr at each step. Edge effects were handled by filling missing values with the nearest valid observations.

2.3. Assessing the Magnitude of Surge Peaks

In the third step, we identify the top 117 independent surge peaks, corresponding to an average of three events per year, using a spatially varying POT. To ensure the independence of the peaks, we apply a uniform declustering time of 72 hr, that is, 36 hr on both sides of the peak (Arns et al., 2013). Next, we analyze the magnitude of surge peaks by computing various descriptive statistics for each output station, such as the mean, coefficient of variation, skewness, and kurtosis.

In addition to the spatially varying POT, we also assess other commonly used extreme value methods, including the annual maxima, r largest (3 events per year), and POT with fixed thresholds (99.5th% and 99.7th%) (Arns et al., 2013; Haigh et al., 2010; Wahl et al., 2017). Although selecting a fixed number of events based on the spatially varying POT may include lower or moderate surges in regions with fewer extreme storm surges, the results from the other extreme value methods are spatially consistent and lead to the same general conclusions (Figure S1 in Supporting Information S1).

2.4. Assessing the Seasonality of Surge Peaks

In the fourth step, we transform the dates, that is, the specific day on which the selected surge peaks occur, into angular values and evaluate their probability distribution type. We first test the null hypothesis of circular uniformity to identify output stations where the surge peak dates follow a uniform distribution, indicating no clear seasonality (Mardia & Jupp, 2009; Pewsey et al., 2013). To do this, we employ four nonparametric tests: Rayleigh's test, Rao spacing test, Kuiper's test, and Watson's goodness of fit test (Jammalamadaka & Sengupta, 2001; Mardia & Jupp, 2009; Pewsey et al., 2013). Following the approach of Veatch and Villarini. (2020), we reject the assumption of uniformity at a significance level of 5% and apply the Bonferroni correction to adjust for multiple comparisons between tests (Bonferroni, 1936). We use this correction to prevent results from incorrectly appearing statistically significant (Weisstein, 2004).

For stations that exhibit statistical significance (i.e., that do not follow a uniform probability distribution), we assess seasonality by fitting the mixture model of the vMF distribution to the angular dates of the surge peaks using the movMF R package (see Banerjee et al., 2005; Hornik & Grün, 2014). Mixture models of the vMF distribution enable the modeling of cyclic data. This is done by representing the overall distribution of the data as a weighted sum of component distributions, each characterized by its direction, effectively capturing clusters in the underlying data (see Hornik & Grün, 2014; Veatch & Villarini, 2020, for a detailed description). The number of components determines how many distributions the mixture model fits to the underlying data. Therefore, we set the number of the vMF components to three. This means that the model fits one to three distributions to the surge peak dates. Subsequently, we determine the number of seasons based on the model distribution with the lowest Bayesian information criterion (BIC) and extract the peak dates of the surge season. We also conduct a sensitivity test with a higher component value and found results consistent with the model choice of three components.

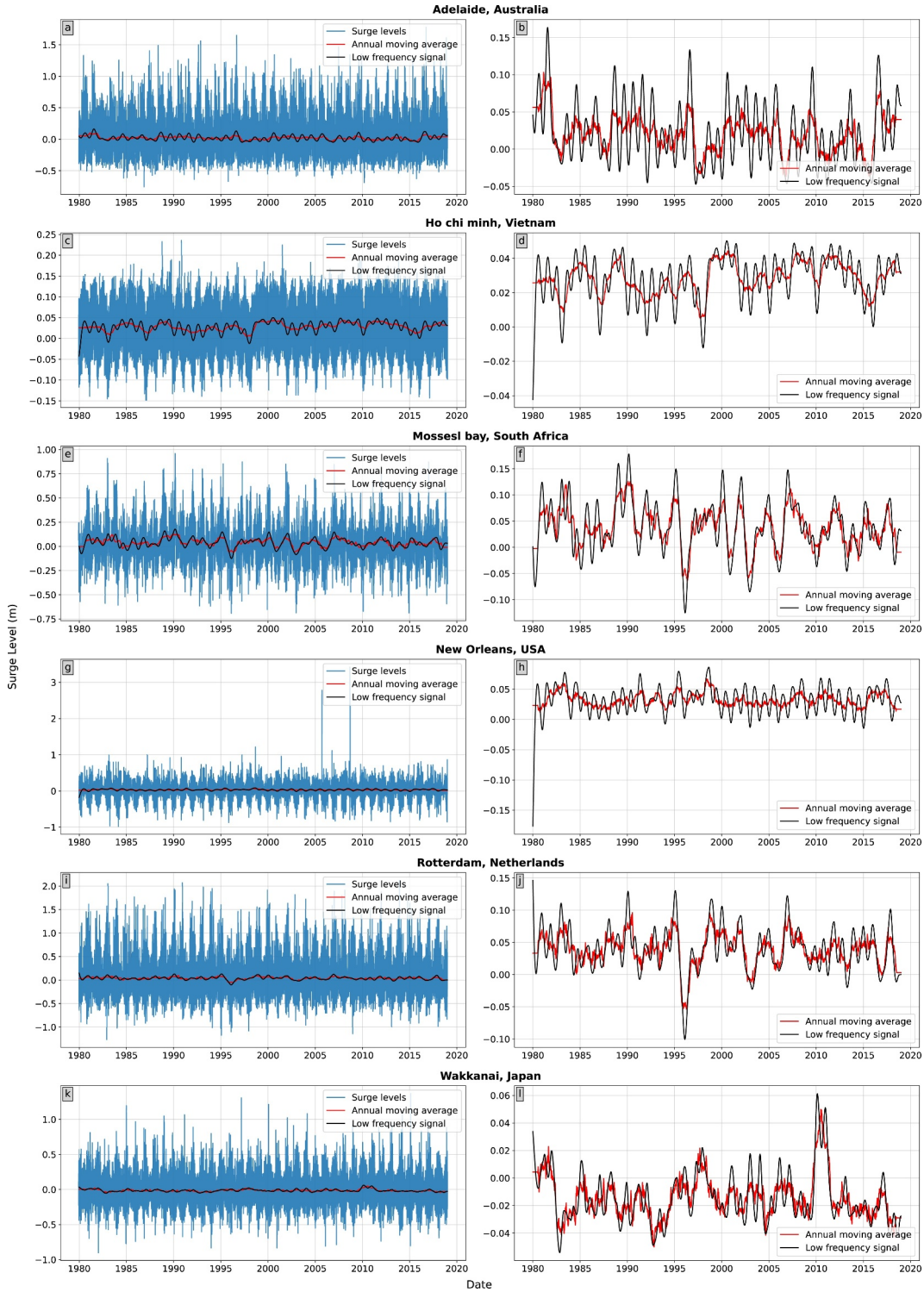

Figure 2. Surge level time series and meteorological trends shown for selected output station. The panels on the left (panels a, c, e, g, i, and k) display surge levels and the meteorological trends, as determined by the low-pass filter (black) and the annual moving average (red). The panels on the right (panels b, d, f, h, j, and l) compare the variation of the trend determined by the low-pass filter (low-frequency signal) with that of the annual moving average.

For stations with more than one season, we rank the seasons according to their mixture proportions, which represent their relative contribution to the overall probability density. The mixture with the highest probability density is interpreted as the primary storm surge season, while the subsequent proportions are referred to as the secondary and minor seasons. Finally, we estimate the length of the surge season by identifying the local extrema (maxima and minima) in the first derivative of the distribution function, which indicates points of the most rapid change in event frequency (Veatch & Villarini, 2022).

We evaluate the performance of the movMF by computing the circular correlation between the quantiles of the observed surge peak dates and the best-fitting model. Given that the result for a mixed distribution is a weighted combination of different distributions, the movMF model lacks theoretical functions for computing model quantiles. Therefore, following the approach of Veatch and Villarini (2022), we adopt the Monte Carlo simulation for estimating the empirical mixture distribution (Figure S6 in Supporting Information S1).

2.5. Validation of GTSM Storm Surge Seasonality Using Tide Gauge Data

To validate the assessment of seasonality derived from the GTSM surge data set, we applied the directional statistical analysis to observed sea levels from tide gauge stations in the Global Extreme Sea Level Analysis (GESLA-3) database (Haigh et al., 2023). The GESLA database provides hourly water level records for 5119 tide gauge stations. However, we use the nontidal residuals for tide gauge stations processed by Martín et al. (2024). This processed data set contains 1485 tide gauge stations. We retain those with data covering an overlapping period from 1981 to 2010, resulting in a subset of 579 tide gauge stations. We further refine this selection by identifying duplicate stations from different data providers and retain only one record from each duplicate. In addition, to ensure consistent comparison, we match each tide gauge station with the nearest modeled output station, retaining only the closest in cases where multiple tide gauge stations match with the same model output station. This process results in a total number of 461 tide gauge stations used for the validation.

3. Results

The result section is organized into two main parts. In the first section, we assess the global characteristics of storm surge seasons, which include the number of seasons, peak dates of the identified season, and the length of the season. It should be noted that this analysis does not distinguish between storm types, which may have influenced the characteristics of storm surge seasons. Rather, it focuses on the most extreme surge peaks and represents periods during which they cluster irrespective of the meteorological driver. In the second section, we assess the frequency and the magnitude of the seasonal surge peaks and synthesize their regional differences to highlight broad spatial patterns, which may have implications for extreme value analysis.

To aid interpretation in the text, we refer to tropical regions as those between 30° north and south of the equator, subtropical regions as those between 30° and 45°, and extratropical regions as those beyond 45°.

3.1. Characteristics of Storm Surge Season

3.1.1. Number of Storm Surge Seasons

First, we analyze the number of storm surge seasons for each output station. Figure 3 shows that about 17% of the output stations lack a distinct season; 56% have one season; 26% have two seasons; and fewer than 2% have three seasons. The density of output stations in Europe and the Mediterranean largely influences the proportion of output stations with one or two seasons. Considering that output stations with three seasons comprise less than 2% of all output stations and are mostly found in the open ocean, we exclude them from our discussion.

Output stations that lack a distinct season are scattered across the globe. However, a clear cluster is evident along the coastlines of the Caribbean, the Gulf of Mexico, the southeastern and southern coasts of South America, Japan, the Philippines, eastern Australia, New Zealand, Papua New Guinea, and many small islands of the Pacific Ocean. This indicates that these areas lack a strong storm surge season. This aligns with findings from Barroso et al. (2024) that showed that these areas have the most significant variation in the timing of storm surges. We tested different extreme value methods (see Section 2.3) and found consistent patterns in regions that lacked a clear surge season (Figure S1 in Supporting Information S1).

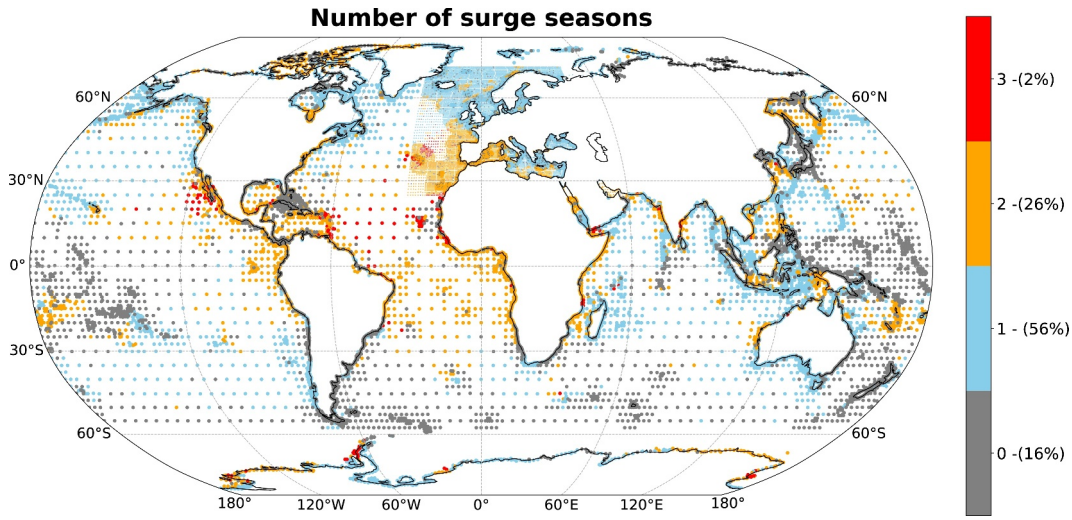

Figure 3. Global map showing the number of storm surge seasons. The numbers (0–3) on the color bar represent the number of seasons, with zero indicating no distinct season. Additionally, the percentage values in brackets represent the proportion of output stations that fall into that category.

We assessed the surge magnitudes in these areas by analyzing the empirical surge peaks (Figure S2 in Supporting Information S1). Our findings indicate that the average surge peak is generally small in these areas, averaging below 0.5 m (Figure S2a in Supporting Information S1). However, the high variability and distribution of surge peaks in Japan reveal that Japan experiences more frequent and intense tropical cyclones than other coastlines without a clear surge season. Additionally, we validated results from the GTSM-ERA5 surge residuals with nontidal residuals from observed sea level records (see Section 2.5). Overall, both data sets show strong agreement (>50%) in the number of seasons except along the Mediterranean, East North America and East Asian coastlines, where agreement is weak (<50%) (Figure S3c in Supporting Information S1). Notably, while observations along the Japanese coastline reveal a distinct surge season, this pattern is not captured in the GTSM-ERA5 surge data set (Figures S3a and S3b in Supporting Information S1). Additionally, mismatches are most pronounced along TC hotspots.

Most parts of Asia, Australia, Europe, and North America typically have one season (Figure 3). In contrast, large parts of Africa and South America experience two seasons, with the notable exceptions of one season in Madagascar, South Africa, and Chile. Additionally, Central America, the East Coast of the United States, Hudson Bay in Canada, Southern Europe, southeast China, South Korea, Western Australia, and coastlines along the Sea of Okhotsk also experience two seasons. The occurrence of two seasons on the East Coast of the United States may be linked to the seasonal regimes of both tropical cyclones and midlatitude storms (Booth et al., 2017; Lobeto et al., 2018).

3.1.2. Peak of the Storm Surge Season

Second, we assess the peak date(s) of the storm surge season(s) (Figure 4). The peak dates, derived by taking the mean of the distribution, represent the average timing of storm surges. Areas with a single storm surge season, located in the extratropical regions of the Northern Hemisphere and the subtropical regions of the Southern Hemisphere, typically experience their peak storm surge season during the winter months of their respective hemispheres, aligning with the midlatitude storm regime. The midlatitude storm regime is influenced by significant temperature gradients (i.e., difference between cold polar air and warm tropical air masses) at the polar front, resulting in severe midlatitude storms (Hall et al., 2015).

In the tropical region of Africa and South America, the surge season peaks between March and May and between September and November in areas with two seasons (Figure 4). One factor that may explain this bimodality is the large-scale meridional movement of the intertropical convergence zone (ITCZ), the tropical low-pressure belt. During the summer months in both hemispheres, the tropical pressure belt shifts toward the hemisphere experiencing warmer temperatures. However, during the transitional months between winter and summer in both

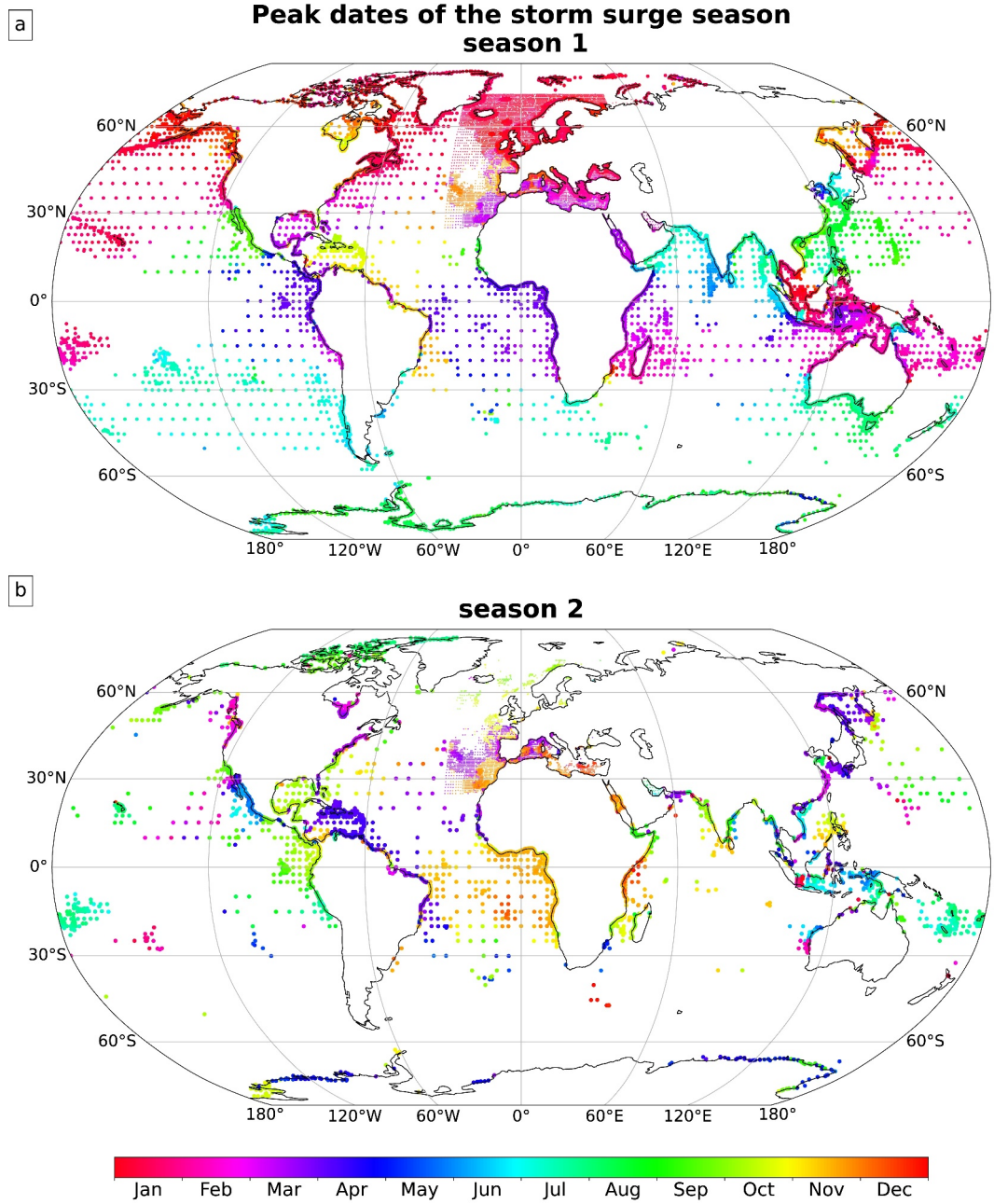

Figure 4. Global map showing the peak dates of the primary and secondary surge season (panels a and b). The peak date represents the average timing of storm surges.

hemispheres, it shifts toward the equator (Bischoff & Schneider, 2016; Lashkari et al., 2017; Schneider et al., 2014). These alternating patterns alter wind circulation and pressure gradients, thereby influencing the timing of surge peaks (Huang & Guan, 2012; Y. Liu et al., 2022; Studholme et al., 2022; Waliser & Gautier, 1993). The influence of this alternating pattern is also evident in the timing of the surge season along the coastlines of Mexico and parts of the Caribbean, where the variability of surge peaks is higher (Figure S1 in Supporting Information S1).

Subtropical regions, such as the East Coast of North America and Southern Europe, also experience two seasons with peak dates associated with the winter and summer storm regimes (Figure 4). In winter, midlatitude storms develop and storm tracks move southward as the polar fronts and the ITCZ shift southward. In summer, TC tracks

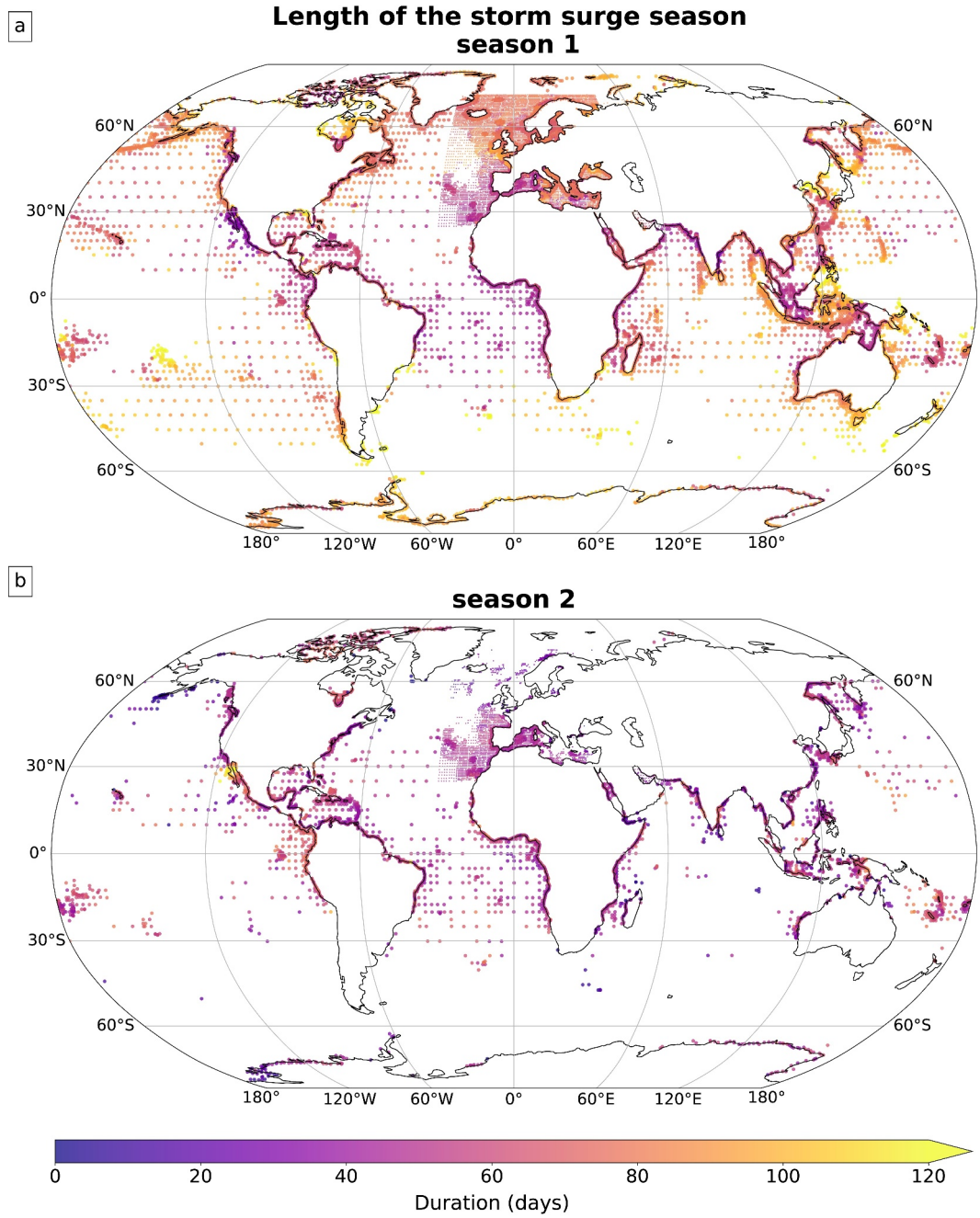

Figure 5. Global map showing the length of the primary and secondary storm surge season (panels a and b).

extend into the subtropics, as the polar front and ITCZ shifts northward (Hall et al., 2015; Schneider et al., 2014; Waliser & Gautier, 1993). As a result, this region is vulnerable to both storm systems since it lies in a critical transition zone. The effect of this phenomenon occurs on the East Coast of North America, where the primary season peaks in winter, aligning with the midlatitude storm regime and the secondary season peaks in summer, aligning with the TC season (Lobeto et al., 2018; Wahl & Chambers, 2015; Zhang et al., 2000).

3.1.3. Length of the Storm Surge Season

Third, we analyze the length of the storm surge season for all output stations with one or two storm surge seasons. The length of the storm surge season refers to the period with the highest likelihood of storm surges. Figures 5a

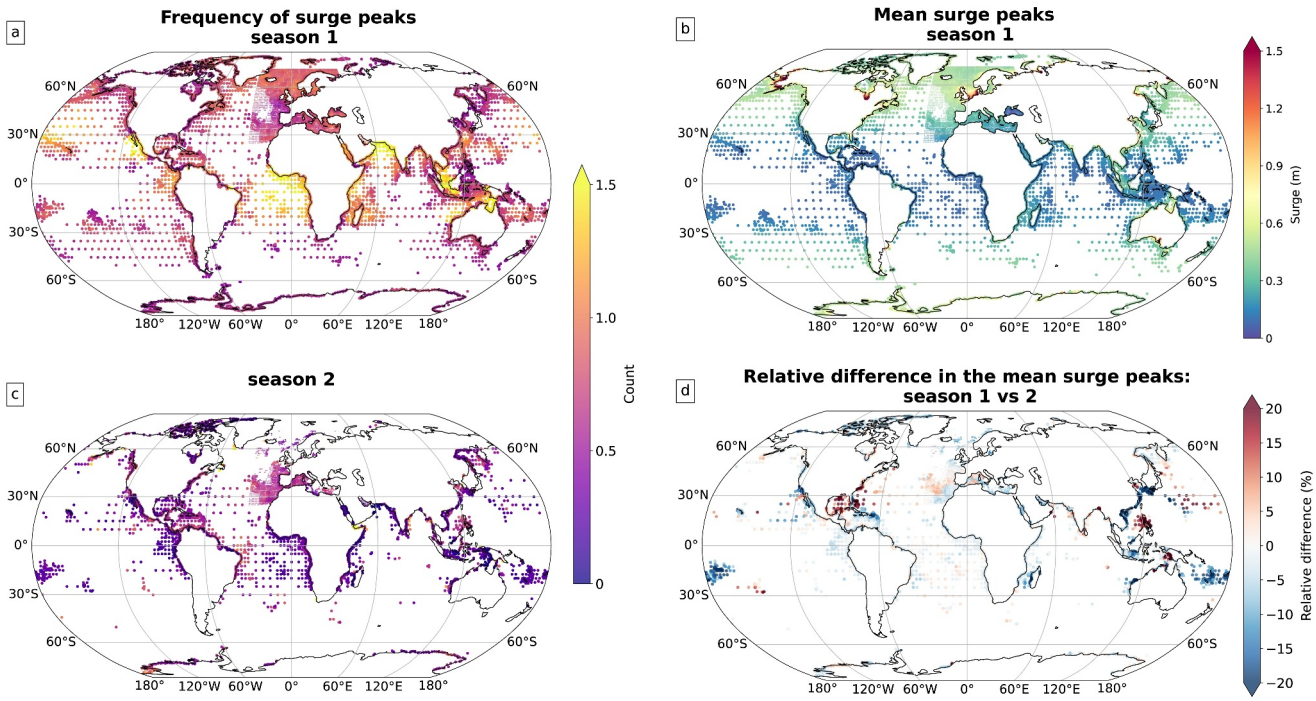

Figure 6. Global map showing the seasonal density of storm surge peaks (panels a and c), the mean magnitude of the surge peaks (panel b), and the relative difference in the mean magnitude of the surge peaks between the primary and the secondary season (panel d). The red (blue) color in panel d indicates larger surges in the secondary (primary) season.

and 5b show that the length of both the primary and secondary seasons is generally less than 120 days for most of the output stations. However, in a few stations scattered across the globe, the duration of the storm surge season exceeds 120 days. These stations are typically located close to areas that lack a strong seasonality (Figure 3).

In areas with one season, the primary season is generally longer, extending beyond 80 days in parts of Europe and Indonesia, the Mediterranean, North-East America, and southern Australia. Conversely, the Gulf of Carpentaria and parts of the coastlines of Southeast Asia are exceptions, with the primary storm surge season lasting between 30 and 45 days (Figure 5a). The short duration of the season suggests that the timing of storm surges in this area is tightly spaced with minimal deviation from the season's peak, which falls in the TC months (Figure 4a).

Areas with two seasons generally have a shorter primary season than areas with one season. In these areas, the primary and secondary seasons are typically less than 80 days with little spatial variability. In the East and West Coasts of the United States, the length of the primary season, which aligns with the midlatitude storm season, is nearly twice the length of the secondary season, which aligns with the tropical cyclones season (Figures 5a and 5b). This indicates greater variability in the timing of surge peaks during the midlatitude storm season than the TC season in these areas.

3.2. Frequency and Magnitude of Seasonal Storm Surge Peaks

3.2.1. Frequency of Seasonal Storm Surge Peaks

We assess the frequency of storm surge peaks for the primary and secondary seasons. The frequency of the storm surge peak was computed by normalizing the number of surge peaks by the season's length. Figures 6a and 6c show that the frequency of surge peaks is generally higher in areas with a single season. This pattern may be explained by the longer duration of the primary season in single-season areas. The highest frequencies exceed one event in the primary season and occur along the coastlines of Madagascar, Pakistan, and India along the Indian Ocean. Similar frequencies occur in Mexico and Queensland and in Southeast Asia, along the Pacific. Notably, these areas also have the shortest storm surge season (Figure 4a). These findings may suggest that the processes

that influence the timing of surge peaks in these areas typically align around the same time and have not significantly deviated over the period of our analysis.

Lower frequencies of storm surge peaks in the primary season occur in areas with two seasons. This includes the coastlines of Africa and South America, where the density of surge events is the lowest (less than 0.5). Significant differences in frequency between the primary and the secondary seasons can be found in the tropical regions of Africa and the coastlines of Ecuador, Peru, and Mexico. In these areas, the frequency of the surge peaks generally exceeds one event in the primary season, with a substantially lower frequency in the secondary season. Although both seasons in these areas have relatively similar lengths, the higher number of surge peaks in the primary season indicates a greater concentration of events in this period.

3.2.2. Magnitude of Seasonal Storm Surge Peaks

Next, we analyze the magnitude of the seasonal storm surge peaks as well as their variability. We do this by computing the mean, coefficient of variation, and skewness and kurtosis of the storm surge peaks within the defined primary and secondary seasons. Figures 6b and 6d show that the largest surges in the primary season generally occur in coastal areas with wide and shallow continental shelves in the extratropical region. These areas include the North Sea in northwestern Europe, the Bering Sea in Alaska, and Hudson Bay in Canada, where the mean surge peak exceeds 1.2 m. In TC-prone areas, such as the Gulf of Carpentaria, Western Australia, and Madagascar, where the frequency of events is high (Figure 5), the mean magnitude of the storm surge peaks is smaller—less than 1 m (Figure 6). This suggests that seasonal surge peaks in these areas are lower, and only a few were caused by tropical cyclones. This is supported by a high coefficient of variation, as shown in Figure S4 in Supporting Information S1.

In some areas with two storm surge seasons, such as the coastlines of East North America, the Philippines, and West Papua, surge magnitudes in the secondary season are higher by more than 20% than those in the primary season. On the East Coast of the United States, the primary season is longer with a higher frequency of surge peaks associated with midlatitude storms (Figures 5, 6a, and 6c). Nonetheless, the mean surge magnitude (Figure 6d) and the coefficient of variation (Figure S4 in Supporting Information S1) indicate that surge peaks associated with midlatitude storms are lower than those from the less frequent but more intense tropical cyclones in the secondary season.

3.2.3. Regional Analysis of Seasonal Distribution of Storm Surge Peaks

Finally, we explore seasonal variations in broader detail and synthesize their regional differences. To do this, we assess the seasonal distribution of surge peaks by aggregating all output stations to the IPCC-AR6 reference regions (Iturbide et al., 2020). The seasonal aggregation of regions are shown in Figure S5 in Supporting Information S1. Results show a clear pattern in the distribution of surge peaks in both seasons (Figure 7). In 26 out of the 29 aggregated regions, the distribution of surge peaks in the primary season is highly skewed to the right, with skewness values ranging from 0.65 in West and central Europe to 4.23 in the Caribbean. This indicates that a few surge peaks in the distribution are extremely large, particularly in the Caribbean. In contrast, the remaining three regions have a near-symmetric distribution with values ranging from −0.24 in southwest South America to 0.45 in West North America. This indicates that the probability of very high surge peaks in these regions is low, which may have implications for model choice for extreme value analysis.

The surge peaks distribution is right-skewed in all 17 regions with two seasons. However, when comparing the primary and secondary seasons, the seasonal distribution varies from region to region (Figure 7). For instance, in northeast North America, only the Arctic region and James Bay in Canada experience two surge seasons (Figure 3). While the reason for the seasonal characteristics and spatial cluster is unclear, the average surge peak in the secondary season is 20% higher than in the primary season (Figure 7a2). In addition, the secondary season has a higher variability of surge peaks with a moderate right skew, which indicates a lower probability of exceptionally high peaks than the primary season. A similar pattern, but with a clear indication of which season poses the most significant risk, can be observed in East North America (Figure 7a4), where the primary season is dominated by midlatitude storms and the secondary season is dominated by tropical cyclones (Booth et al., 2017; Lobeto et al., 2018). The average surge magnitude is similar in both seasons, with surge peak distributions highly skewed to the right. However, the secondary season has more exceptionally high peaks and a higher variability in surge peak distribution, as shown by the higher right skew and the coefficient of variation (Figure 7a4). This

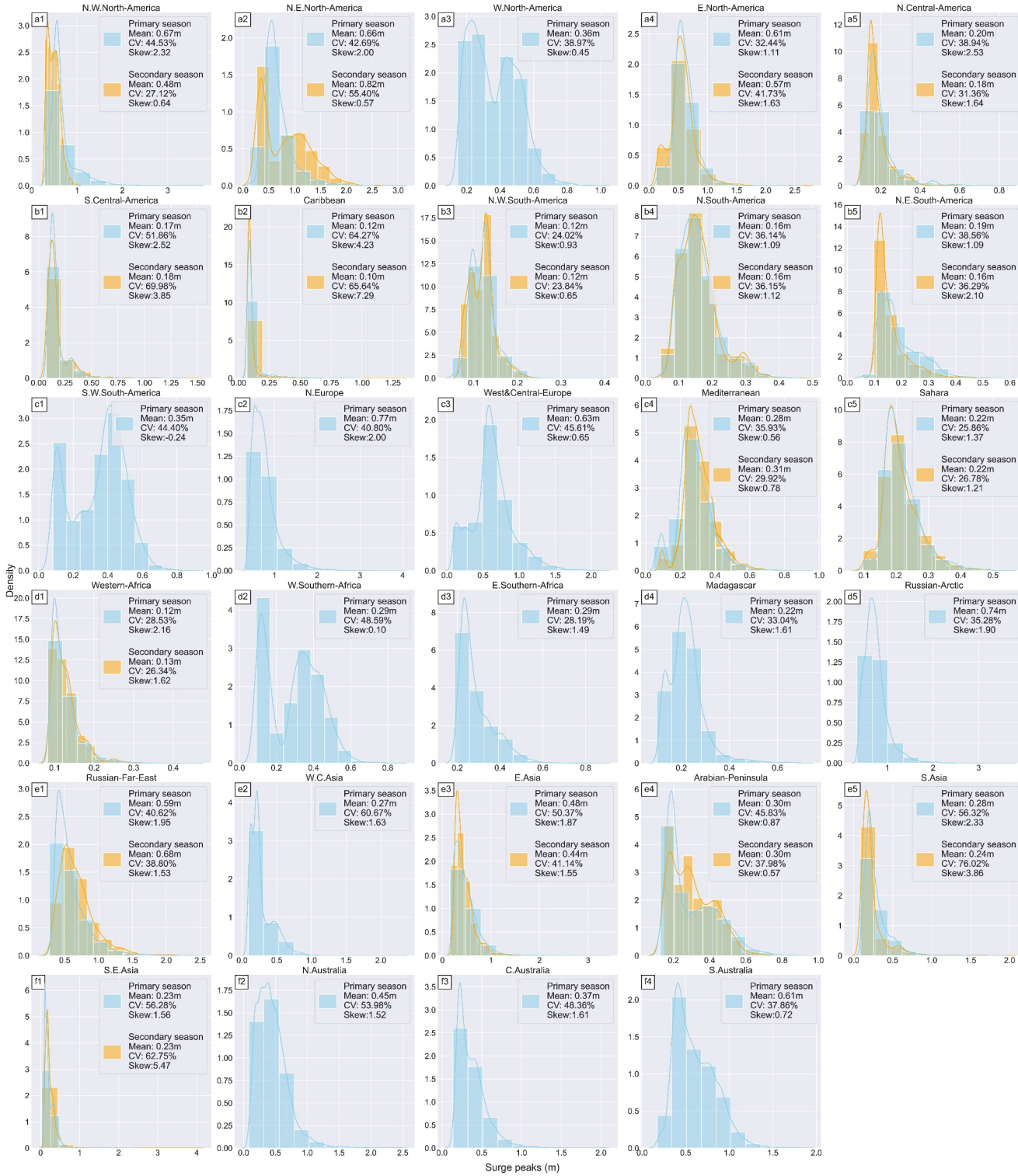

Figure 7. Global seasonal distribution of surge peaks aggregated to the IPCC reference regions. The histogram bars and the kernel density lines show the distribution of storm surge peaks for the primary (sky blue) and the secondary season (orange).

implies that surge peaks in the TC season may return higher surge levels for rare events than when the two seasons are combined, as the inclusion of the lower skew may reduce the overall tail heaviness.

4. Discussion

4.1. Implications for Coastal Risk Assessment

This study analyzed storm surge seasonality based on hourly surge data from a global hydrodynamic model with full coverage of coastal areas. It complements previous global studies that have used tide gauge data or satellite data (Barroso et al., 2024; Bij de Vaate et al., 2024; Menéndez & Woodworth, 2010). While previous global studies have primarily used nonstationary extreme value models based on monthly maxima, we use directional statistics with a mixture model to identify multiple seasons. Our results reveal that extreme storm surge season is not necessarily confined to a single, well-defined period across the globe. Notably, we found that nearly half of the global coastal stations, predominantly in tropical and subtropical regions, either lack a distinct surge season or experience heightened surge activity across multiple periods. For regions with well-defined seasons, our results provide insights into when extreme storm surges are most frequent and the average magnitudes of surge peaks in this period. This information is particularly useful for designing and maintaining coastal infrastructure, enhancing early warning systems, and evaluating risk insurance (Miura et al., 2021; Trace-Kleeberg et al., 2023). In addition, regions with multiple surge seasons or those lacking a distinct seasonal pattern may require adjustments to their flood preparedness plans. Specifically, regions with multiple surge seasons may need to account for the impact of secondary windows, especially if this season coincides with other flood-generating mechanisms. Likewise, areas that lack a clear surge season may need to extend their preparedness measures over longer timeframes due to the uncertainty in the timing of surge peaks.

Climate change may drive changes in storm surge seasonality, potentially altering the timing of surge peaks (Reinert et al., 2021; Roustan et al., 2022). Moreover, the occurrence of extreme sea level (ESL) is also influenced by variations in waves, tides, and mean sea level (Idier et al., 2019; Kirezci et al., 2020; Marcos et al., 2019; Vitousek et al., 2017; Vousdoukas et al., 2018), all of which exhibit seasonal cycles (Barroso et al., 2025; Tsimplis & Woodworth, 1994). For effective risk management, it would be relevant to assess the seasonality of other ESL components and possible long-term shifts (Vanem, 2015), as the cooccurrence of seasonal peaks may significantly amplify total water levels.

4.2. Comparison With Previous Global Studies

When comparing our research with previous global studies (Barroso et al., 2024; Bij de Vaate et al., 2024; Menéndez & Woodworth, 2010), results about the peak of the storm surge season are largely consistent. However, there are two main areas for further discussion. First, our results highlight the importance of circular uniformity tests and challenge the use of single models in directional statistics, which generally obscures multimodal distributions (Cunderlik et al., 2004a; Mardia & Jupp, 2009; Pewsey et al., 2013). For instance, our results indicate no clear seasonality in the Gulf of Mexico, which contrasts with Barroso et al. (2024), who reported a clear winter season. This contrast may be due to the omission of the circular uniformity test in their analysis. Likewise, in regions like the East North America, where we identified two surge seasons associated with tropical and mid-latitude storms, our results do not fully agree with Barroso et al. (2024), who identified only the winter season based on applying directional statistics with a single model.

Second, our analysis provides valuable insights on incorporating semiannual cycles in nonstationary extreme value analysis (NEVA) (Coles, 2001), especially in regions with two seasons (Méndez et al., 2007). For instance, in locations with a single, well-defined storm surge season, our findings complement previous works on nonstationarity (Bij de Vaate et al., 2024; Menéndez & Woodworth, 2010), showing that the month when storm surge frequency peaks is also the month with the highest probability of extreme storm surges. However, in regions with two seasons, our results do not fully align. This contrast may be linked to variations in the distribution parameters of the NEVA or methodical differences in selecting extreme values. Approaches based on block maxima, commonly used in NEVA, provide sufficient temporal variability for model parameters to vary over time (Reinert et al., 2021; Vanem, 2015; Wahl & Chambers, 2015, 2016). However, as highlighted by Méndez et al. (2007); omitting the semiannual cycle from the parameters of the model distribution may underestimate variability in locations with multiple seasonal cycles. This is further supported by the harmonic analysis of Barroso et al. (2024), which showed monsoonal regions exhibit strong semiannual cycles, reinforcing

the need to consider them in NEVA. Moreover, the use of monthly maxima may also obscure the repetitive timing of the most extreme events, which methods like the POT and r largest capture effectively. Therefore, it would be relevant to explore nonstationary approaches based on other extreme value selection (Serafin & Ruggiero, 2014).

4.3. Limitations

Our analysis has a number of limitations. First, our analysis is based on the GTSM-ERA5 data set from 1980 to 2018, a 39-year period that reflects the near-present-day climate. Although this data set has been shown to accurately represent extreme sea levels (Dullaart et al., 2021; Muis et al., 2023), the data set contains biases in the surface winds, especially for extreme conditions (Belmonte Rivas & Stoffelen, 2019; Campos et al., 2022) and underestimates the intensification of tropical cyclones (Malakar et al., 2020). These biases can result in inaccuracies not only in the magnitude of storm surges but also in their timing. Although these biases may significantly underestimate the magnitude of extreme storm surges, particularly for tropical cyclones (Dullaart et al., 2021), we do not expect significant biases in seasonality (Chen et al., 2024; Molina et al., 2021). However, given the discrepancy in the number of seasons between the modeled and observed surge data sets, particularly along the Japanese coastline, our results in areas prone to tropical cyclones may be affected by spatial and temporal biases in the ERA5 reanalysis data, as the most extreme cases of TC intensification are not captured in the ERA5 reanalysis (Belmonte Rivas & Stoffelen, 2019; Malakar et al., 2020). In addition, our results in areas prone to tropical cyclones, such as the Gulf of Mexico, may be affected by the fact that tropical cyclones are rarer, which limits their occurrence within the 39-year period of our analysis. Future work could address this by applying our method to larger data ensembles (e.g., Benito et al., 2025; Bloemendaal et al., 2020), focusing the analysis on more extreme events. This would also enable the assessment of seasonal return periods, which have practical relevance for insurance assessment.

Second, there are uncertainties associated with the statistical methods used. We use the spatially varying POT method to select extreme events, resulting in a fixed number of surge peaks (Arns et al., 2013; Haigh et al., 2010). The optimal threshold for extreme event selections varies depending on local characteristics (Arns et al., 2013; Wahl et al., 2017). A threshold that is too low results in the inclusion of events that are not extreme, which could dilute the seasonal characteristics captured by the vMF distribution. For instance, the inclusion of moderate extremes may affect the number of seasons, extend the length of the storm surge season, or even shift the surge peak dates. Additionally, the use of equally sized windows to identify independent extremes does not account for important local variations in storm duration (Martín et al., 2024). Future studies could explore whether accounting for local variations in the statistical parameters may improve our results.

Third, there are inherent uncertainties associated with the use of mixture models and directional statistics. For single-component models, quantile-quantile computation provides a means to easily measure uncertainty and assess model fit (Pewsey et al., 2013). However, for mixture models, such as the vMF distribution, the absence of theoretical functions to compute the quantiles for mixture distributions makes it difficult to accurately assess model performance (Veatch & Villarini, 2022). We use the Monte Carlo simulation-based method to assess model performance and estimate uncertainty. However, the uncertainty estimates from such simulation-based approaches are not entirely reliable, which limits broader applications of mixture models. Future studies could explore or develop alternative performance metrics suitable for mixture distributions. In addition, we statistically define the length of the storm surge season based on the first derivative of the distribution function, following Veatch and Villarini (2022). One limitation to this approach is that some extreme peaks may occur just outside the boundaries of the derivative's window, excluding significant events. Future studies could explore alternative definitions of the start and the end of the storm surge season, such as those proposed by Chen et al. (2013), Cunderlik et al. (2004b), P. Liu et al. (2010), and Ouarda et al. (1993).

5. Conclusions and Outlook

Using hourly surge data from 1980 to 2018 from a global hydrodynamic model, this study examined storm surge seasonality, providing valuable insights for regions that lack observations from tide gauges. We applied directional statistics and fit a mixture model based of the vMF distribution, enabling a comprehensive assessment of spatiotemporal variability in storm surge seasonality. Compared to previous global studies that employed nonstationary extreme value models, our statistical approach has the advantage of identifying multiple seasons.

Our results show that nearly half of the global coastal stations, predominantly in tropical and subtropical regions, either lack a distinct surge season or experience heightened surge activity across multiple periods. While these patterns may have been recognized locally, our results reveal a consistent large-scale spatial pattern linked to regional atmospheric patterns. By comparing the primary and secondary seasons, we show that differences in the length of surge seasons are minimal in regions with bimodal surge seasons; however, the seasonal surge peaks differ, particularly on the East Coast of the United States, associated with the TC storm regime. Moreover, our results reveal that while the seasonality of storm surges, globally, is strongest in TC-prone coastlines such as India, Madagascar, and Pakistan, it is weakest but biased in the Gulf of Mexico and the Japanese and the Caribbean coastlines. This contrast provides insight into the complex atmospheric-oceanic interaction that influences the occurrence of tropical cyclones in these regions. Additionally, by aggregating coastlines into distinct regions, our results show that the seasonal distribution of surge peaks varies by regions and reflects the associated risks of the underlying storm regime. For instance, along the east coasts of North America, although the winter storms typically produce higher surges, the most extreme surges are most likely to occur during the TC season.

We conclude with suggestions for future research based on the results presented and discussed in this study. Model validation revealed biases, particularly along TC-prone areas, such as Japan and the Gulf of Mexico, for a 30-year period. Future studies could leverage longer storm surge time series, extending the observation period, especially in areas prone to tropical cyclones, which has a low probability of occurrence, to improve the reliability of our results. Additionally, a longer time series would enable the assessment of temporal trends in storm surge seasons influenced by interannual variability or historical climate change. Moreover, it would be interesting to apply our methodology to future climate scenarios to investigate how storm surge seasonality is represented in global climate models and how the seasons may change under a warmer climate. Future research could also investigate the seasonality of other extreme sea levels components (i.e., mean sea level, waves, and tides) to identify the probability of cooccurrence.

Conflict of Interest

The authors declare no conflicts of interest relevant to this study.

Data Availability Statement

The GTSM-ERA5 surge data used in this study are openly available at the C3S Climate Data Store via 10.24381/cds.a6d42d60. The IPCC regional classification data used in this study are openly available via https://doi.org/10.5194/ESSD-12-2959-2020. The codes used in the analysis of this paper are available https://github.com/Apolola/storm_surge_seasonality and on Zenodo https://doi.org/10.5281/zenodo.17218661.

Acknowledgments

This research is part of the Climate cHange impActs on extreme sea levels iN Coastal watErs (CHANCE) project, which is financed by the Dutch Research Council (NWO) under the Grant OCENW.M.21.109 (SM, JAA). The authors acknowledge that this research was achieved through the Snellius supercomputational resources provided by SURF (http://www.surf.nl).

References

Arns, A., Wahl, T., Haigh, I. D., Jensen, J., & Pattiaratchi, C. (2013). Estimating extreme water level probabilities: A comparison of the direct methods and recommendations for best practise. *Coastal Engineering*, *81*, 51–66. https://doi.org/10.1016/j.coastaleng.2013.07.003

Banerjee, A., Dhillon, I. S., Ghosh, J., & Sra, S. (2005). Clustering on the unit hypersphere using von Mises-Fisher distributions.

Barroso, A., Wahl, T., Enríquez, A. R., Morim, J., & Dangendorf, S. (2025). Changes in the seasonal cycle of storm surge along the global coastline. *Journal of Geophysical Research: Oceans*, *130*(5), e2024JC022187. https://doi.org/10.1029/2024JC022187

Barroso, A., Wahl, T., Li, S., Enriquez, A., Morim, J., Dangendorf, S., et al. (2024). Observed spatiotemporal variability in the annual sea level cycle along the global coast. *Journal of Geophysical Research: Oceans*, *129*(4), e2023JC020300. https://doi.org/10.1029/2023JC020300

Belmonte Rivas, M., & Stoffelen, A. (2019). Characterizing ERA-interim and ERA5 surface wind biases using ASCAT. *Ocean Science*, *15*(3), 831–852. https://doi.org/10.5194/os-15-831-2019

Benito, I., Eilander, D., Kelder, T., Ward, P. J., Aerts, J. C. J. H., & Muis, S. (2025). Pooling seasonal forecast ensembles to estimate storm tide return periods in extra-tropical regions. *Journal of Geophysical Research: Oceans*, *130*(8), e2025JC022614. https://doi.org/10.1029/2025JC022614

Bij de Vaate, I., Slobbe, D. C., & Verlaan, M. (2024). Mapping the spatiotemporal variability in global storm surge water levels using satellite radar altimetry. *Ocean Dynamics*, *74*(3), 169–182. https://doi.org/10.1007/s10236-023-01596-2

Bischoff, T., & Schneider, T. (2016). The equatorial energy balance, ITCZ position, and double-ITCZ bifurcations. *Journal of Climate*, *29*(8), 2997–3013. https://doi.org/10.1175/JCLI-D-15-0328.1

Bloemendaal, N., Haigh, I. D., de Moel, H., Muis, S., Haarsma, R. J., & Aerts, J. C. J. H. (2020). Generation of a global synthetic tropical cyclone hazard dataset using STORM. *Scientific Data*, *7*(1), 40. https://doi.org/10.1038/s41597-020-0381-2

Bonferroni, C. (1936). *Teoria statistica delle classi e calcolo delle probabilita* (Vol. 8, pp. 3–62). Pubblicazioni del R istituto superiore di scienze economiche e commericiali di firenze.

Booth, J. F., Kwon, Y.-O., Ko, S., Small, R. J., & Msadek, R. (2017). Spatial patterns and intensity of the surface storm tracks in CMIP5 models. *Journal of Climate*, *30*(13), 4965–4981. https://doi.org/10.1175/JCLI-D-16-0228.1

Calafat, F. M., Wahl, T., Tadesse, M. G., & Sparrow, S. N. (2022). Trends in Europe storm surge extremes match the rate of sea-level rise. *Nature*, *603*(7903), 841–845. https://doi.org/10.1038/s41586-022-04426-5

Campos, R. M., Gramcianinov, C. B., de Camargo, R., & da Silva Dias, P. L. (2022). Assessment and calibration of ERA5 severe winds in the Atlantic Ocean using satellite data. *Remote Sensing*, *14*(19), 19. https://doi.org/10.3390/rs14194918

Chen, L., Singh, V. P., Guo, S., Fang, B., & Liu, P. (2013). A new method for identification of flood seasons using directional statistics. *Hydrological Sciences Journal*, *58*(1), 28–40. https://doi.org/10.1080/02626667.2012.743661

Chen, T.-C., Collet, F., & Di Luca, A. (2024). Evaluation of ERA5 precipitation and 10-m wind speed associated with extratropical cyclones using station data over North America. *International Journal of Climatology*, *44*(3), 729–747. https://doi.org/10.1002/joc.8339

Coles, S. (2001). *An introduction to statistical modeling of extreme values*. Springer.

Copernicus Climate Change Service [C3S]. (2022). ERA5: Fifth generation of ECMWF atmospheric reanalyses of the global climate. Retrieved from https://cds.climate.copernicus.eu/cdsapp#!/home

Cunderlik, J. M., Ouarda, T. B. M. J., & Bobée, B. (2004a). Determination of flood seasonality from hydrological records/Détermination de la saisonnalité des crues à partir de séries hydrologiques. *Hydrological Sciences Journal*, *49*(3), 11. https://doi.org/10.1623/hysj.49.3.511.54351

Cunderlik, J. M., Ouarda, T. B. M. J., & Bobée, B. (2004b). On the objective identification of flood seasons. *Water Resources Research*, *40*(1). https://doi.org/10.1029/2003WR002295

Dhakal, N., Jain, S., Gray, A., Dandy, M., & Stancioff, E. (2015). Nonstationarity in seasonality of extreme precipitation: A nonparametric circular statistical approach and its application. *Water Resources Research*, *51*(6), 4499–4515. https://doi.org/10.1002/2014WR016399

Dullaart, J. C., Muis, S., Bloemendaal, N., & Aerts, J. C. (2020). Advancing global storm surge modelling using the new ERA5 climate reanalysis. *Climate Dynamics*, *54*(1–2), 1007–1021. https://doi.org/10.1007/s00382-019-05044-0

Dullaart, J. C. M., Muis, S., Bloemendaal, N., Chertova, M. V., Couasnon, A., & Aerts, J. C. J. H. (2021). Accounting for tropical cyclones more than doubles the global population exposed to low-probability coastal flooding. *Communications Earth & Environment*, *2*(1), 1. https://doi.org/10.1038/s43247-021-00204-9

Fernández-Montblanc, T., Vousdoukas, M. I., Mentaschi, L., & Ciavola, P. (2020). A Pan-European high resolution storm surge hindcast. *Environment International*, *135*, 105367. https://doi.org/10.1016/j.envint.2019.105367

Haigh, I. D., Marcos, M., Talke, S. A., Woodworth, P. L., Hunter, J. R., Hague, B. S., et al. (2023). GESLA version 3: A major update to the global higher-frequency sea-level dataset. *Geoscience Data Journal*, *10*(3), 293–314. https://doi.org/10.1002/gdj3.174

Haigh, I. D., Nicholls, R., & Wells, N. (2010). A comparison of the main methods for estimating probabilities of extreme still water levels. *Coastal Engineering*, *57*(9), 838–849. https://doi.org/10.1016/j.coastaleng.2010.04.002

Hall, R., Erdélyi, R., Hanna, E., Jones, J. M., & Scaife, A. A. (2015). Drivers of North Atlantic polar front jet stream variability. *International Journal of Climatology*, *35*(8), 1697–1720. https://doi.org/10.1002/joc.4121

Hermans, T. H. J., Le Bars, D., Katsman, C. A., Camargo, C. M. L., Gerkema, T., Calafat, F. M., et al. (2020). Drivers of interannual sea level variability on the Northwestern European Shelf. *Journal of Geophysical Research: Oceans*, *125*(10), e2020JC016325. https://doi.org/10.1029/2020JC016325

Hersbach, H., Bell, B., Berrisford, P., Hirahara, S., Horányi, A., Muñoz-Sabater, J., et al. (2020). The ERA5 global reanalysis. *Quarterly Journal of the Royal Meteorological Society*, *146*(730), 1999–2049. https://doi.org/10.1002/qj.3803

Hornik, K., & Grün, B. (2014). movMF: An R package for fitting mixtures of von Mises-Fisher distributions. *Journal of Statistical Software*, *58*(10), 1–31. https://doi.org/10.18637/jss.v058.i10

Huang, Q., & Guan, Y. (2012). Does the Asian monsoon modulate tropical cyclone activity over the South China Sea? *Chinese Journal of Oceanology and Limnology*, *30*(6), 960–965. https://doi.org/10.1007/s00343-012-1273-x

Idier, D., Bertin, X., Thompson, P., & Pickering, M. D. (2019). Interactions between mean sea level, tide, surge, waves and flooding: Mechanisms and contributions to sea level variations at the coast. *Surveys in Geophysics*, *40*(6), 1603–1630. https://doi.org/10.1007/s10712-019-09549-5

Iturbide, M., Gutiérrez, J. M., Alves, L. M., Bedia, J., Cerezo-Mota, R., Cimadevilla, E., et al. (2020). An update of IPCC climate reference regions for subcontinental analysis of climate model data: Definition and aggregated datasets. *Earth System Science Data*, *12*(4), 2959–2970. https://doi.org/10.5194/essd-12-2959-2020

Jammalamadaka, S. R., & Sengupta, A. (2001). Topics in circular statistics. *World Scientific*.

Kernkamp, H. W. J., Van Dam, A., Stelling, G. S., & de Goede, E. D. (2011). Efficient scheme for the shallow water equations on unstructured grids with application to the Continental Shelf. *Ocean Dynamics*, *61*(8), 1175–1188. https://doi.org/10.1007/s10236-011-0423-6

Kirezci, E., Young, I. R., Ranasinghe, R., Muis, S., Nicholls, R. J., Lincke, D., & Hinkel, J. (2020). Projections of global-scale extreme sea levels and resulting episodic coastal flooding over the 21st century. *Scientific Reports*, *10*(1), 11629. https://doi.org/10.1038/s41598-020-67736-6

Lashkari, H., Mohammadi, Z., & Keikhosravi, G. (2017). Annual fluctuations and displacements of inter tropical Convergence Zone (ITCZ) within the range of Atlantic Ocean-India. *Open Journal of Ecology*, *7*(1), 1–33. https://doi.org/10.4236/oje.2017.71002

Liu, P., Guo, S., Xiong, L., & Chen, L. (2010). Flood season segmentation based on the probability change-point analysis technique. *Hydrological Sciences Journal – Journal Des Sciences Hydrologiques*, *55*(4), 540–554. https://doi.org/10.1080/02626667.2010.481087

Liu, Y., Cai, W., Lin, X., & Li, Z. (2022). Increased extreme swings of Atlantic intertropical convergence zone in a warming climate. *Nature Climate Change*, *12*(9), 828–833. https://doi.org/10.1038/s41558-022-01445-y

Lobeto, H., Menendez, M., & Losada, I. J. (2018). Toward a methodology for estimating coastal extreme sea levels from satellite altimetry. *Journal of Geophysical Research: Oceans*, *123*(11), 8284–8298. https://doi.org/10.1029/2018JC014487

Lowe, R. J., Cuttler, M. V. W., & Hansen, J. E. (2021). Climatic drivers of extreme sea level events along the coastline of Western Australia. *Earth's Future*, *9*(4), e2020EF001620. https://doi.org/10.1029/2020EF001620

Malakar, P., Kesarkar, A. P., Bhate, J. N., Singh, V., & Deshamukhya, A. (2020). Comparison of reanalysis data sets to comprehend the evolution of tropical cyclones over North Indian Ocean. *Earth and Space Science*, *7*(2), e2019EA000978. https://doi.org/10.1029/2019EA000978

Mäll, M., Suursaar, Ü., Nakamura, R., & Shibayama, T. (2017). Modelling a storm surge under future climate scenarios: Case study of extra-tropical cyclone Gudrun (2005). *Natural Hazards*, *89*(3), 1119–1144. https://doi.org/10.1007/s11069-017-3011-3

Marcos, M., Calafat, F. M., Berihuete, Á., & Dangendorf, S. (2015). Long-term variations in global sea level extremes. *Journal of Geophysical Research: Oceans*, *120*(12), 8115–8134. https://doi.org/10.1002/2015JC011173

Marcos, M., Rohmer, J., Vousdoukas, M. I., Mentaschi, L., Le Cozannet, G., & Amores, A. (2019). Increased extreme coastal water levels due to the combined action of storm surges and wind waves. *Geophysical Research Letters*, *46*(8), 4356–4364. https://doi.org/10.1029/2019GL082599

Mardia, K. V., & Jupp, P. E. (2009). *Directional statistics*. John Wiley & Sons.

Martín, A., Wahl, T., Enriquez, A. R., & Jane, R. (2024). Storm surge time series de-clustering using correlation analysis. *Weather and Climate Extremes*, *45*, 100701. https://doi.org/10.1016/j.wace.2024.100701

Mawdsley, R. J., & Haigh, I. D. (2016). Spatial and temporal variability and long-term trends in Skew surges globally. *Frontiers in Marine Science*, *3*. https://doi.org/10.3389/fmars.2016.00029

Mcinnes, K. L., Walsh, K. J. E., Hubbert, G. D., & Beer, T. (2003). Impact of sea-level rise and storm surges on a coastal community. *Natural Hazards*, *30*(2), 187–207. https://doi.org/10.1023/A:1026118417752

Méndez, F. J., Menéndez, M., Luceño, A., & Losada, I. J. (2007). Analyzing monthly extreme sea levels with a time-dependent GEV model. https://doi.org/10.1175/JTECH2009.1

Menéndez, M., & Woodworth, P. L. (2010). Changes in extreme high water levels based on a quasi-global tide-gauge data set. *Journal of Geophysical Research*, *115*(C10). https://doi.org/10.1029/2009jc005997

Mester, B., Vogt, T., Bryant, S., Otto, C., Frieler, K., & Schewe, J. (2023). Human displacements from tropical cyclone Idai attributable to climate change. *Natural Hazards and Earth System Sciences*, *23*(11), 3467–3485. https://doi.org/10.5194/nhess-23-3467-2023

Miura, Y., Qureshi, H., Ryoo, C., Dinenis, P. C., Li, J., Mandli, K. T., et al. (2021). A methodological framework for determining an optimal coastal protection strategy against storm surges and sea level rise. *Natural Hazards*, *107*(2), 1821–1843. https://doi.org/10.1007/s11069-021-04661-5

Molina, M. O., Gutiérrez, C., & Sánchez, E. (2021). Comparison of ERA5 surface wind speed climatologies over Europe with observations from the HadISD dataset. *International Journal of Climatology*, *41*(10), 4864–4878. https://doi.org/10.1002/joc.7103

Muis, S., Aerts, J. C. J. H., Antolínez, J. A. A., Dullaart, J. C., Duong, T. M., Erikson, L., et al. (2023). Global projections of storm surges using high-resolution CMIP6 climate models. *Earth's Future*, *11*(9), e2023EF003479. https://doi.org/10.1029/2023EF003479

Muis, S., Apecechea, M. I., Dullaart, J., de Lima Rego, J., Madsen, K. S., Su, J., et al. (2020). A high-resolution global dataset of extreme sea levels, tides, and storm surges, including future projections. *Frontiers in Marine Science*, *7*, 263. https://doi.org/10.3389/fmars.2020.00263

Muis, S., Haigh, I. D., Guimarães Nobre, G., Aerts, J. C. J. H., & Ward, P. J. (2018). Influence of El niño-southern oscillation on global coastal flooding. *Earth's Future*, *6*(9), 1311–1322. https://doi.org/10.1029/2018EF000909

Muis, S., Verlaan, M., Winsemius, H. C., Aerts, J. C., & Ward, P. J. (2016). A global reanalysis of storm surges and extreme sea levels. *Nature Communications*, *7*(1), 11969. https://doi.org/10.1038/ncomms11969

Naeije, M. C. (2022). Radar altimeter database system [Data archive]. Retrieved from http://rads.tudelft.nl

Needham, H. F., & Keim, B. D. (2012). A storm surge database for the US Gulf Coast. *International Journal of Climatology*, *32*(14), 2108–2123. https://doi.org/10.1002/joc.2425

Nicholls, R. J. (2006). "Storm surges in coastal areas." Natural disaster hotspots, case studies, the World Bank hazard management unit, disaster risk management series *6*. 79–108.

Ouarda, T., Ashkar, F., & El-Jabi, N. (1993). Peaks over threshold model for seasonal flood variations. Proceedings of the Symposium on Engineering Hydrology, 341–346.

Parajka, J., Kohnová, S., Bálint, G., Barbuc, M., Borga, M., Claps, P., et al. (2010). Seasonal characteristics of flood regimes across the Alpine-Carpathian range. *Journal of Hydrology*, *394*(1–2), 78–89. https://doi.org/10.1016/j.jhydrol.2010.05.015

Parker, K., Erikson, L., Thomas, J., Nederhoff, K., Barnard, P., & Muis, S. (2023). Relative contributions of water-level components to extreme water levels along the US Southeast Atlantic Coast from a regional-scale water-level hindcast. *Natural Hazards*, *117*(3), 2219–2248. https://doi.org/10.1007/s11069-023-05939-6

Petterson, J. S., Stanley, L. D., Glazier, E., & Philipp, J. (2006). A preliminary assessment of social and economic impacts associated with Hurricane Katrina. *American Anthropologist*, *108*(4), 643–670. https://doi.org/10.1525/aa.2006.108.4.643

Pewsey, A., Neuhäuser, M., & Ruxton, G. D. (2013). *Circular statistics in R*. OUP Oxford.

Pugh, D., & Woodworth, P. L. (2014). *Sea-level science: Understanding tides, surges, tsunamis and mean sea-level changes*. Cambridge University Press.

Reinert, M., Pineau-Guillou, L., Raillard, N., & Chapron, B. (2021). Seasonal shift in storm surges at brest revealed by extreme value analysis. *Journal of Geophysical Research: Oceans*, *126*(12), e2021JC017794. https://doi.org/10.1029/2021jc017794

Roberts, J., & Roberts, T. D. (1978). Use of the Butterworth low-pass filter for oceanographic data. *Journal of Geophysical Research*, *83*(C11), 5510–5514. https://doi.org/10.1029/JC083iC11p05510

Roustan, J.-B., Pineau-Guillou, L., Chapron, B., Raillard, N., & Reinert, M. (2022). Shift of the storm surge season in Europe due to climate variability. *Scientific Reports*, *12*(1), 1–11. https://doi.org/10.1038/s41598-022-12356-5

Rueda, A., Vitousek, S., Camus, P., Tomás, A., Espejo, A., Losada, I. J., et al. (2017). A global classification of coastal flood hazard climates associated with large-scale oceanographic forcing. *Scientific Reports*, *7*(1), 5038. https://doi.org/10.1038/s41598-017-05090-w

Schneider, T., Bischoff, T., & Haug, G. H. (2014). Migrations and dynamics of the intertropical convergence zone. *Nature*, *513*(7516), 45–53. https://doi.org/10.1038/nature13636

Serafin, K. A., & Ruggiero, P. (2014). Simulating extreme total water levels using a time-dependent, extreme value approach. *Journal of Geophysical Research: Oceans*, *119*(9), 6305–6329. https://doi.org/10.1002/2014JC010093

Studholme, J., Fedorov, A. V., Gulev, S. K., Emanuel, K., & Hodges, K. (2022). Poleward expansion of tropical cyclone latitudes in warming climates. *Nature Geoscience*, *15*(1), 14–28. https://doi.org/10.1038/s41561-021-00859-1

Trace-Kleeberg, S., Haigh, I. D., Walraven, M., & Gourvenec, S. (2023). How should storm surge barrier maintenance strategies be changed in light of sea-level rise? A case study. *Coastal Engineering*, *184*, 104336. https://doi.org/10.1016/j.coastaleng.2023.104336

Tsimplis, M. N., & Woodworth, P. L. (1994). The global distribution of the seasonal sea level cycle calculated from coastal tide gauge data. *Journal of Geophysical Research*, *99*(C8), 16031–16039. https://doi.org/10.1029/94JC01115

Vanem, E. (2015). Non-stationary extreme value models to account for trends and shifts in the extreme wave climate due to climate change. *Applied Ocean Research*, *52*, 201–211. https://doi.org/10.1016/j.apor.2015.06.010

Veatch, W., & Villarini, G. (2020). Modeling the seasonality of extreme coastal water levels with mixtures of circular probability density functions. *Theoretical and Applied Climatology*, *140*(3), 1199–1206. https://doi.org/10.1007/s00704-020-03143-1

Veatch, W., & Villarini, G. (2022). Modeling riverine flood seasonality with mixtures of circular probability density functions. *Journal of Hydrology*, *613*, 128330. https://doi.org/10.1016/j.jhydrol.2022.128330

Vitousek, S., Barnard, P. L., Fletcher, C. H., Frazer, N., Erikson, L., & Storlazzi, C. D. (2017). Doubling of coastal flooding frequency within decades due to sea-level rise. *Scientific Reports*, *7*(1), 1399. https://doi.org/10.1038/s41598-017-01362-7

Vousdoukas, M. I., Mentaschi, L., Voukouvalas, E., Verlaan, M., Jevrejeva, S., Jackson, L. P., & Feyen, L. (2018). Global probabilistic projections of extreme sea levels show intensification of coastal flood hazard. *Nature Communications*, *9*(1), 2360. https://doi.org/10.1038/s41467-018-04692-w

Wahl, T., & Chambers, D. P. (2015). Evidence for multidecadal variability in US extreme sea level records. *Journal of Geophysical Research: Oceans*, *120*(3), 1527–1544. https://doi.org/10.1002/2014JC010443

Wahl, T., & Chambers, D. P. (2016). Climate controls multidecadal variability in US extreme sea level records. *Journal of Geophysical Research: Oceans*, *121*(2), 1274–1290. https://doi.org/10.1002/2015JC011057

Wahl, T., Haigh, I. D., Nicholls, R. J., Arns, A., Dangendorf, S., Hinkel, J., & Slangen, A. B. A. (2017). Understanding extreme sea levels for broad-scale coastal impact and adaptation analysis. *Nature Communications*, *8*(1), 16075. https://doi.org/10.1038/ncomms16075

Waliser, D. E., & Gautier, C. (1993). A satellite-derived climatology of the ITCZ. *Journal of Climate*, *6*(11), 2162–2174. https://doi.org/10.1175/1520-0442(1993)006<2162:asdcot>2.0.co;2

Weather Underground. (2025). Weather underground. Retrieved from https://www.wunderground.com/hurricane/articles/2005-hurricane-season-records

Weisstein, E. W. (2004). Bonferroni correction. Retrieved from https://mathworld.wolfram.com/

Woodworth, P. L., Melet, A., Marcos, M., Ray, R. D., Wöppelmann, G., Sasaki, Y. N., et al. (2019). Forcing factors affecting sea level changes at the coast. *Surveys in Geophysics*, *40*(6), 1351–1397. https://doi.org/10.1007/s10712-019-09531-1

Wu, W., Westra, S., & Leonard, M. (2017). A basis function approach for exploring the seasonal and spatial features of storm surge events. *Geophysical Research Letters*, *44*(14), 7356–7365. https://doi.org/10.1002/2017GL074357

Zhang, K., Douglas, B. C., & Leatherman, S. P. (2000). Twentieth-century storm activity along the U.S. East Coast. *Journal of Climate*, *13*(10), 1748–1761. https://doi.org/10.1175/1520-0442(2000)013<1748:tcsaat>2.0.co;2